

A Wideband Circularly Polarized Dielectric Resonator Antenna with Filtering Response

Chuanyun Wang, Xiaofeng Jiang*, Weikang Hu, Qilei Fan, and Jianjun Huang

School of Information Engineering, East China Jiaotong University, Nanchang 330013, China

ABSTRACT: In this paper, a wideband circularly polarized (CP) filtering dielectric resonator antenna (FDRA) is proposed. The proposed antenna consists of a microstrip-Y-shaped slot line coupled feeding structure and a grooved DRA. The Y-shaped slot line not only serves as an energy coupling structure to excite the orthogonal modes (TE_{111}^x mode and TE_{111}^y mode) of DRA, forming the CP radiation effect, but also generates two resonant modes, thereby broadening the antenna impedance bandwidth. In addition, due to the groove engraved on the diagonal of the DRA top wall, the antenna CP performance within the passband is enhanced. Finally, by loading a shorting stub and a spur line on the microstrip feedline, radiation nulls are generated on both sides of the antenna passband, resulting in a quasi-elliptical filter response in the antenna gain curve. To further verify the performance of the antenna design, a prototype CP FDRA is fabricated and measured. The measurement results indicate that the antenna achieves a -10 dB impedance bandwidth of 46.1% (2.67–4.27 GHz) and an axial ratio (AR) bandwidth of 23% (3.08–3.88 GHz), with an average measured gain of approximately 4.9 dBi. This antenna exhibits high-frequency selectivity and an out-of-band suppression level exceeding 10 dB.

1. INTRODUCTION

With the rapid advancement of wireless communication technology, increasingly high demands are being placed on the radio frequency (RF) front-end. Filters and antennas, essential elements of the RF front end, are typically designed independently in communication systems, which no doubt increases the size of the communication device and introduces additional insertion loss because of matching circuits. Filtering antennas, which combine the filtering characteristics of filters with the radiation capabilities of antennas, can reduce the number of devices in a system, thereby enhancing system integration and performance [1, 2]. In recent years, dielectric resonator antennas (DRAs) have emerged as an optimal choice for modern wireless communications due to their inherent advantages of compact size, high radiation efficiency, and absence of surface wave excitation [3, 4]. Therefore, the study of filtering DRAs has received extensive attention in the past few decades [5, 6].

There are primarily two approaches to realize filtering DRAs. One is the synthesis design method, wherein the antenna radiation element is treated as the last resonator of the filter. This method predominantly focuses on the filter design, resulting in superior filtering performance [7–9]. However, the introduction of additional filters or filtering networks inevitably leads to a reduction in antenna gain, and insertion loss remains inevitable. The other is the fusion design method, which focuses on the antenna design and achieves filtering functionality by introducing parasitic elements such as slot lines [10], coupling lines [11], and shorting vias [12] in the feeding network or within the antenna structure itself. This method does not require external filters or filtering networks, avoiding increases

in antenna size and additional insertion loss. However, most of the reported filtering DRAs were linearly polarized (LP), which cannot satisfy the application of complex scenarios.

Compared to linearly polarized (LP) antennas, circularly polarized (CP) antennas are widely recognized in various wireless communication systems for their enhanced capabilities in suppressing multipath fading, reducing polarization mismatch, and offering strong interference resistance. Therefore, it is of great significance to study DRA with CP characteristics. The realization of CP in DRAs is commonly achieved through two techniques: multi-feed and single-feed [13]. It is observed that multi-feed technology can provide a broader axial ratio (AR) bandwidth, but the use of external hybrid couplers or power dividers is required, which inevitably increases the overall size, loss, and complexity of the antenna system [14–16]. In contrast, the single-feed techniques, which obtain CP fields by slightly modifying the shape of the DR, using a specific feed structure, or adding parasitic strips, typically have a simpler feed network but a narrower AR bandwidth of less than 10% [17–19]. As a result, the enhancement of the AR bandwidth in single-feed CP DRAs has become a focal research point among scholars. In [20], a single-feed wideband CP DRA was proposed. A wide AR bandwidth was achieved by introducing four vertical metallic plates surrounding the DR, resulting in three contiguous AR passbands due to the cross-slot-fed DRA, the rotation of the metallic plate, and the interaction between the DR and the metallic plate. In [21], a multilayer comb-like structure was fabricated on the top of the DRA using 3D printing technology to generate CP fields. To expand the bandwidth of the DRA, three dielectric strips were integrated inside the DRA to excite multiple transverse electric (TE) DRA modes. In [22], inside the DR, a 2×2 distributed patch is inserted,

* Corresponding author: Xiaofeng Jiang (xiao_feng202112@163.com).

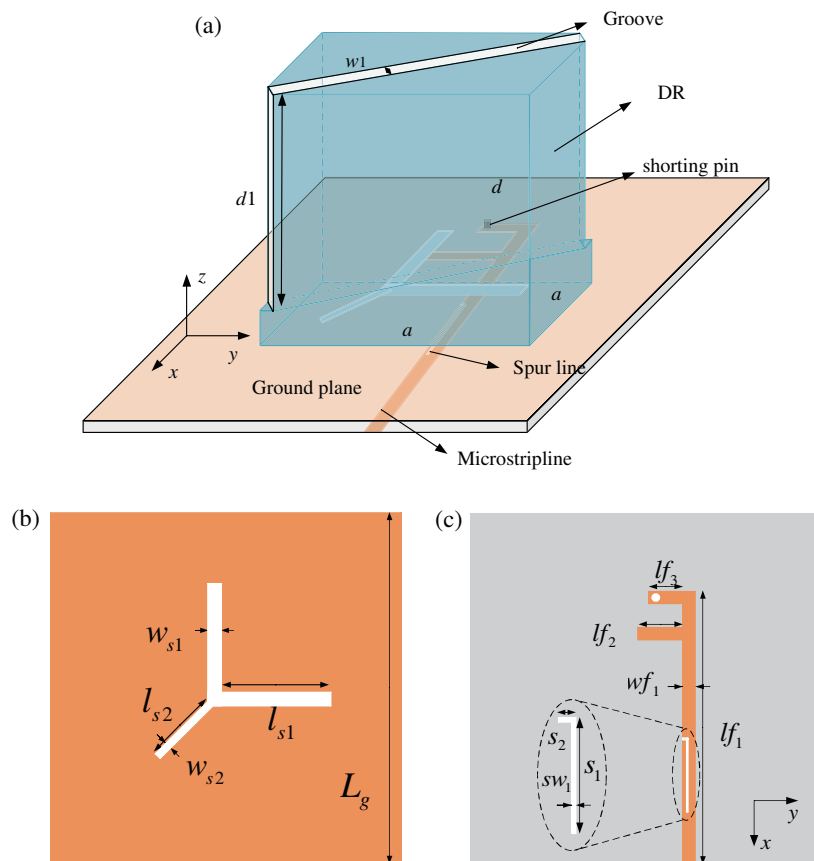


FIGURE 1. Configuration of the proposed wideband CP FDRA. (a) 3D views. (b) Slotline view. (c) Bottom view.

merging the distributed patch mode, DR mode, and the cross-slot mode inside the DRA to achieve the broadband CP effect. In [23], an S-shaped coupling slot is utilized to excite the antenna for generating CP radiation. This is achieved by integrating super-ellipsoidalaxicon dielectric lens on top of the dielectric horn, aimed at enhancing the gain of the DRA as well as its impedance and axial ratio bandwidths. However, the majority of reported DRA studies have focused on either CP or filtering effects [24–26]. Integrating both CP and filtering functions within a DRA presents a significant challenge, as this requires satisfying multiple design parameters simultaneously, such as return loss, AR, radiation pattern, and out-of-band suppression. Therefore, the study of CP DRAs with filtering remains a significant obstacle.

In this paper, a wideband CP DRA with a filtering response is proposed. Bandwidth enhancement and CP radiation have been achieved by utilizing a Y-shaped slot line resonator as a coupling structure. Furthermore, the CP performance of the antenna has been improved within the passband due to the grooves carved on the diagonal of the DRA top wall. Finally, a filtering response is realized by loading a spur line and a shorting stub in the microstrip feedline, which generate two radiation nulls at the passband edges. Simulation and measurement results demonstrate an impedance bandwidth of 46%, an AR bandwidth of 23%, and an in-band flat gain of 4.9 dBi.

2. ANTENNA DESIGN

2.1. Antenna Structure

The geometric layout of the proposed CP FDRA is depicted in Fig. 1. A grooved DRA with a relative permittivity of $\epsilon_{r1} = 10$ is placed on the ground, and a feeding network composed of Y-shaped slot lines and a microstrip feedline is fabricated on an FR4 substrate, characterized by a relative permittivity of $\epsilon_{r2} = 4.4$ and a thickness of $h = 0.8$ mm. The Y-shaped slot lines are located above the substrate, while the $50\ \Omega$ microstrip feedline is printed on the opposite side of the substrate. A shorting stub is loaded on the microstrip feedline with an etched spur line. The design was optimized using ANSYS HFSS software, and detailed parameters of the antenna are presented in Table 1.

TABLE 1. Main design parameters of antenna (mm).

g	a	b	d	h	l_{s1}	l_{s2}	l_{f1}	l_{f2}
40	20.8	20.8	15.5	0.8	11	6.7	25	5
l_{f3}	w_{s1}	w_{s2}	w_{f1}	s_1	s_2	sw_1	d_1	w_1
3.5	1	0.6	1.5	9.2	0.3	0.2	13.8	2

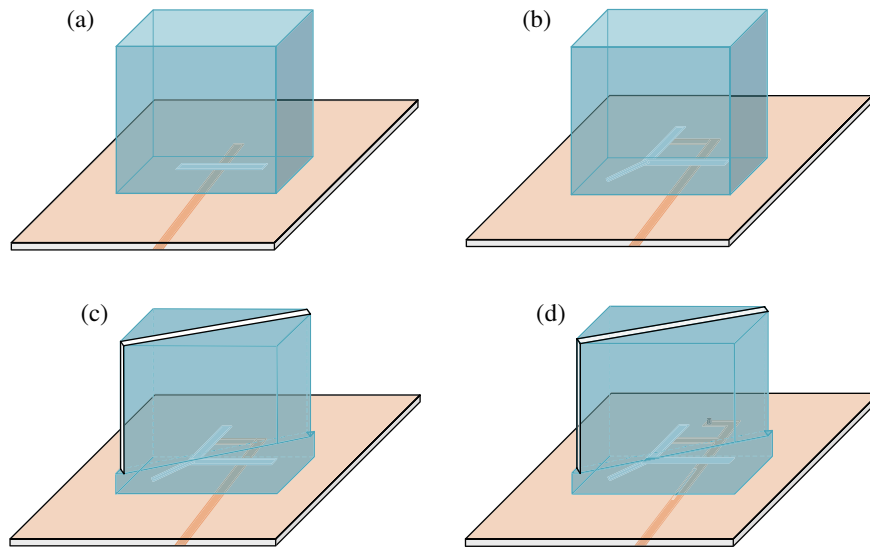


FIGURE 2. Antenna configurations. (a) Antenna I; (b) Antenna II; (c) Antenna III; (d) Proposed antenna.

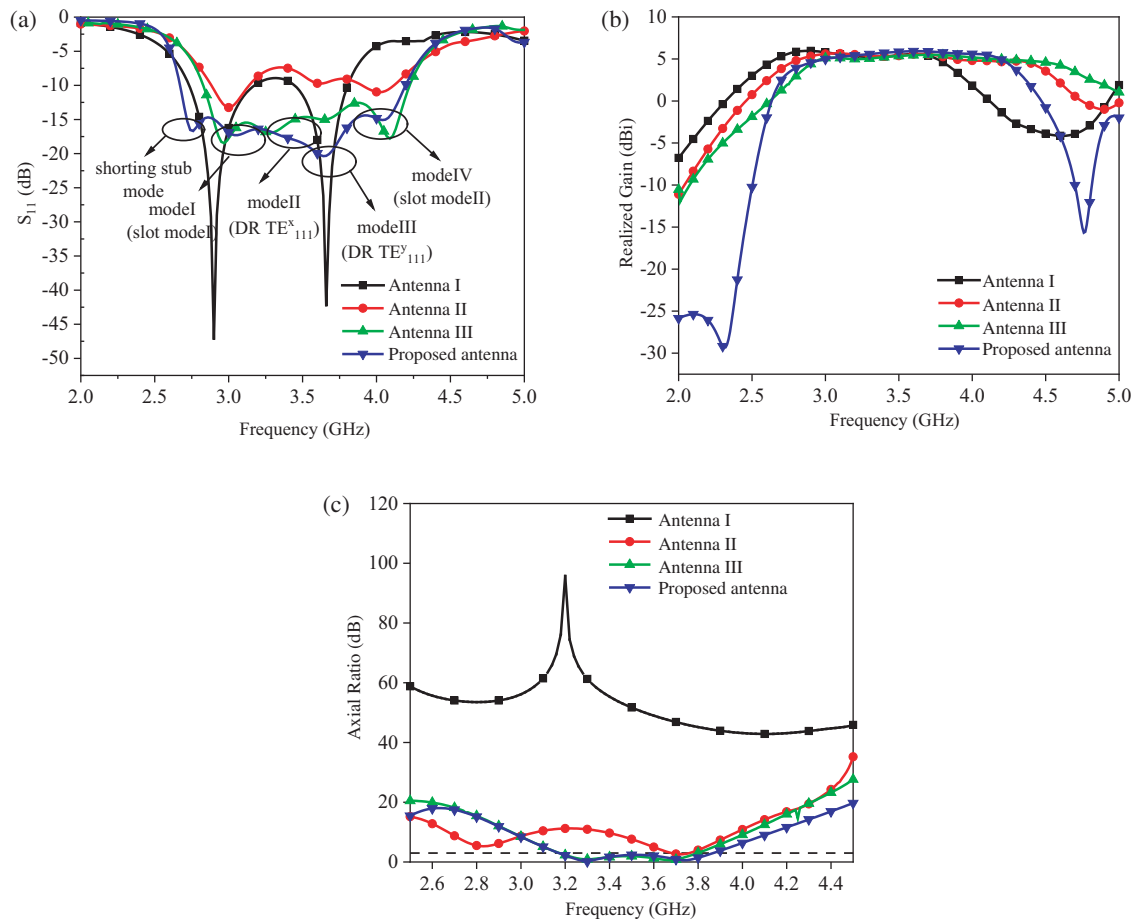


FIGURE 3. Simulation results of the reference and proposed antennas. (a) Reflection coefficient S_{11} . (b) Realized gain and (c) AR.

2.2. Design Procedure

To elucidate the working principle of the proposed CP FDRA, a comparative analysis is conducted on three reference antennas. Fig. 2 illustrates the configurations of the four antennas, and

Fig. 3 presents the simulated S_{11} parameters, realized gains, and axial ratios (ARs). To simplify the comparison, the parameters of these four antennas are kept consistent with those in Table 1. The conventional DRA (antenna I), shown in Fig. 2(a),

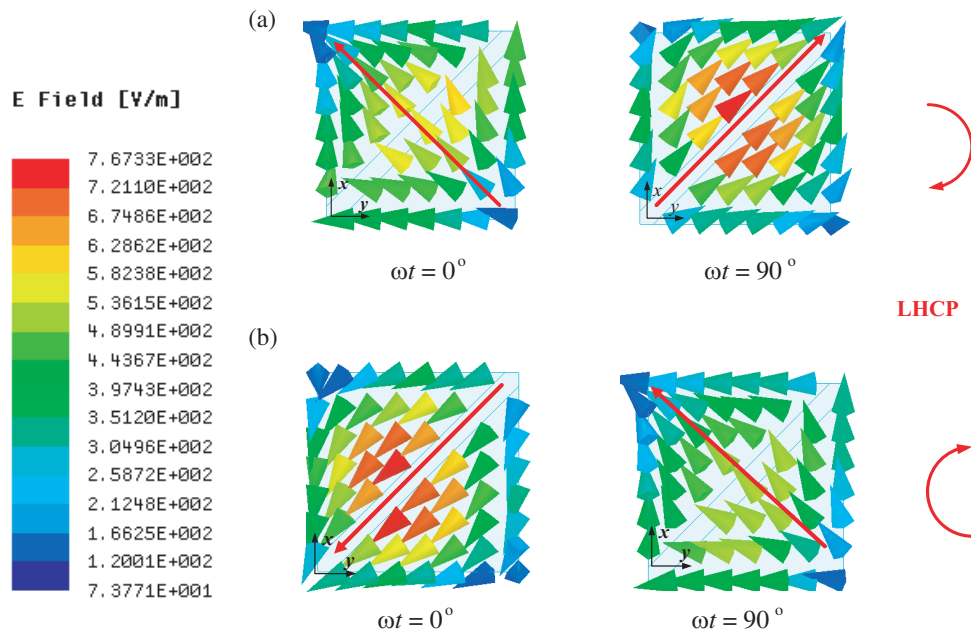


FIGURE 4. Simulated half-period ($\omega t = 0^\circ$ and $\omega t = 90^\circ$) electric field distribution. (a) 2.8 GHz. (b) 3.7 GHz.

which serves as a reference point, consists of a rectangular DRA, a coupling slot, and a microstrip feedline. As shown in Fig. 3, antenna I exhibits two resonant modes within its passband, corresponding to the coupling slot mode and the fundamental mode of the DRA (TE_{111}^y mode). However, the application of the conventional rectangular DRA is limited due to its narrow bandwidth and lack of CP and filtering function to suppress interference signals.

To introduce CP radiation, a Y-shaped slot line is introduced in antenna II to replace the traditional coupling slot of antenna I. Four resonant modes are successfully excited within the passband, as demonstrated by the red solid line in Fig. 3. Mode I and mode IV are attributed to the Y-shaped slot line, while mode II and mode III are the orthogonal modes (TE_{111}^x mode and TE_{111}^y mode) of the DRA, which achieves the CP effect. To further investigate the CP characteristics, Fig. 4 shows the half-period ($\omega t = 0^\circ$ and $\omega t = 90^\circ$) electric field distributions on the top surface of the DRA for the proposed antenna at 2.8 and 3.7 GHz frequencies. It is observed that the current rotates clockwise with the increase in time phase. Therefore, the left-handed circular polarization (LHCP) radiation is realized at 2.8 and 3.7 GHz, respectively. Nonetheless, the CP bandwidth of antenna II remains narrow and lacks a filtering function. In antenna III, perturbations in the internal electric field are induced by carving notches on the diagonal of the DRA top wall, thereby the antenna CP performance within the passband is enhanced, as indicated by the green solid line in Fig. 3(c). Finally, to avoid interference with Wi-Fi, LTE wireless communication systems, and radar systems (such as weather radar and air traffic control), a shorting stub and spur line are loaded onto the microstrip feedline of antenna III to achieve the proposed antenna configuration, as shown in Fig. 2(d). As indicated by the blue solid line in Fig. 3(b), this modification successfully introduced two radiation nulls at 2.3 GHz and 4.7 GHz, significantly enhancing the

antenna out-of-band selectivity. Notably, the loaded shorting stub produced an unexpected resonant mode at 2.7 GHz, which not only further extended the antenna bandwidth but also had no adverse effect on its CP performance.

2.3. Parameter Analysis

As illustrated in Fig. 3, an additional resonant mode at 2.7 GHz is introduced by a shorting stub loaded onto antenna III. To avoid the interference of the shorting stub mode with others and to more accurately explain the operational modes of slot line and DRA, a modal analysis is conducted based on antenna III. As shown in Fig. 5(a), the operating bandwidth of DRA has four resonant modes when $l_{s1} = 11$ mm. As l_{s1} increases, modes I and IV shift toward lower frequencies, while the other two modes exhibit no discernible frequency changes and only have a slight impact on their impedance matching. In Fig. 5(b), an increase in l_{s2} results in the downward frequency shift of modes II and IV, and also the other two modes remain stable. Fig. 6(a) demonstrates that as the groove depth d_l increases, only mode II trends towards higher frequencies, while the remaining three modes are not affected. These observations suggest that modes I and IV correspond to the Y-shaped slot line while modes II and III represent the orthogonal modes of the DRA.

Then, to further verify that the resonant mode at 2.7 GHz is introduced by the loaded shorting stub, a parametric analysis of the shorting stub length lf_3 is carried out. As illustrated in Fig. 7, the shorting stub mode shifts towards lower frequencies with the increase in lf_3 , while the other four modes exhibit no significant frequency shift, affecting only the impedance matching slightly. Therefore, it is confirmed that the loaded shorting stub introduces an additional resonant mode at 2.7 GHz, thereby further enhancing the antenna bandwidth.

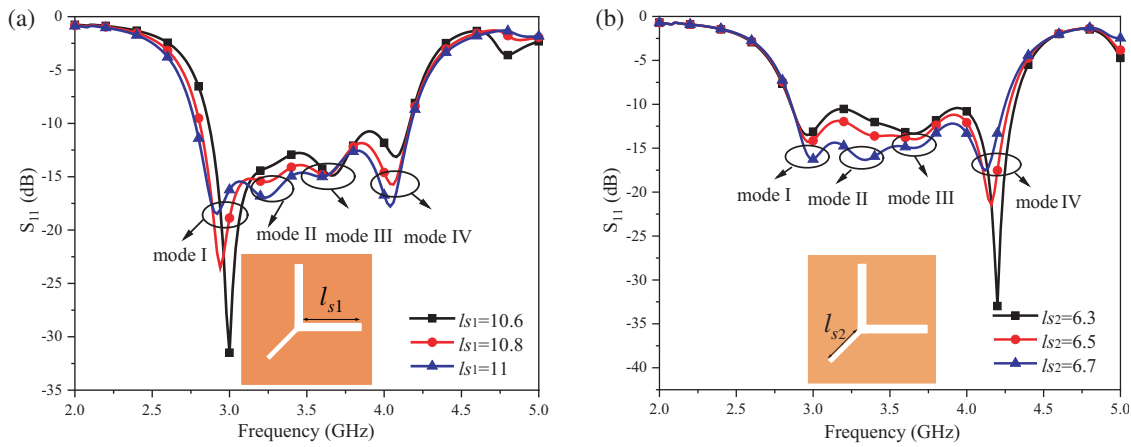


FIGURE 5. (a) Variation of S_{11} with changing l_{11} . (b) Variation of S_{11} with changing l_2 .

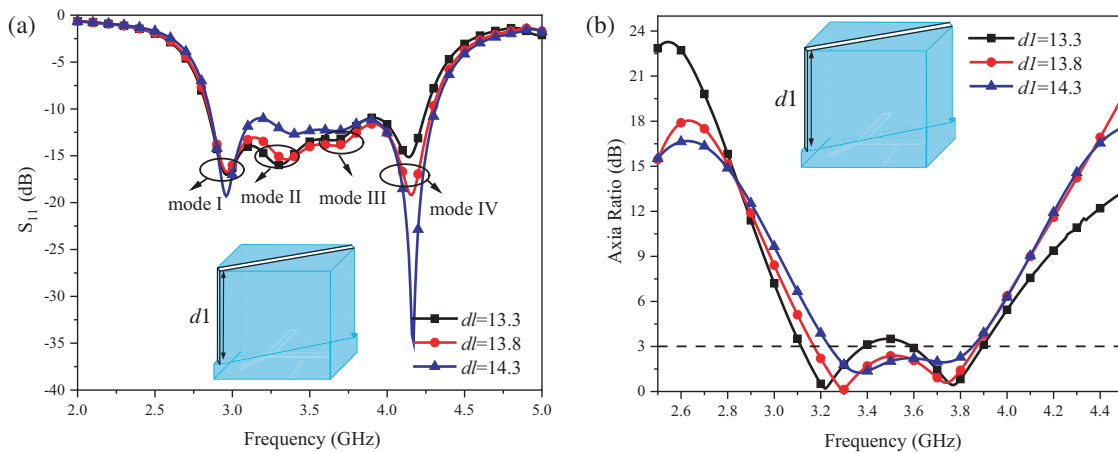


FIGURE 6. Variation of S_{11} and AR with changing dl (a) S_{11} . (b) AR.

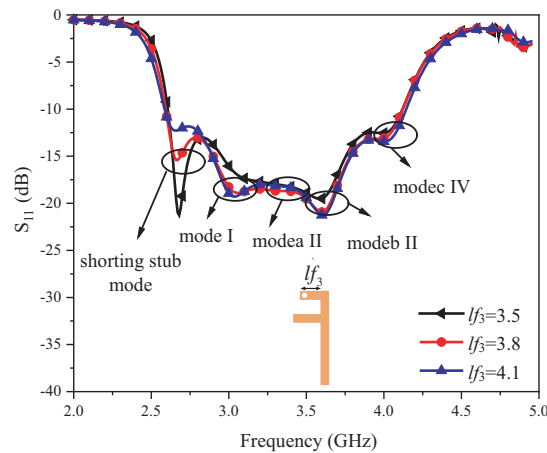


FIGURE 7. Variation of S_{11} with changing lf_3 .

Simultaneously, the radiation nulls significantly contribute to enhancing the out-of-band selectivity of the DRA. Delving into the radiation nulls mechanism of the antenna, Fig. 8 shows that the radiation null f_{n1} originates from the introduced shorting stub, while f_{n2} is a result of the added spur lines. As shown in Fig. 8(a), the radiation null f_{n1} shifts towards lower fre-

quencies with the gradual increase in the length of the shorting stub lf_3 , while the radiation null f_{n2} remains unchanged. Similarly, as illustrated in Fig. 8(b), the radiation null f_{n2} progressively shifts to lower frequencies with the gradual increase in the length of the spur line s_1 , while the radiation null f_{n1} remains unchanged, which meets expectations.

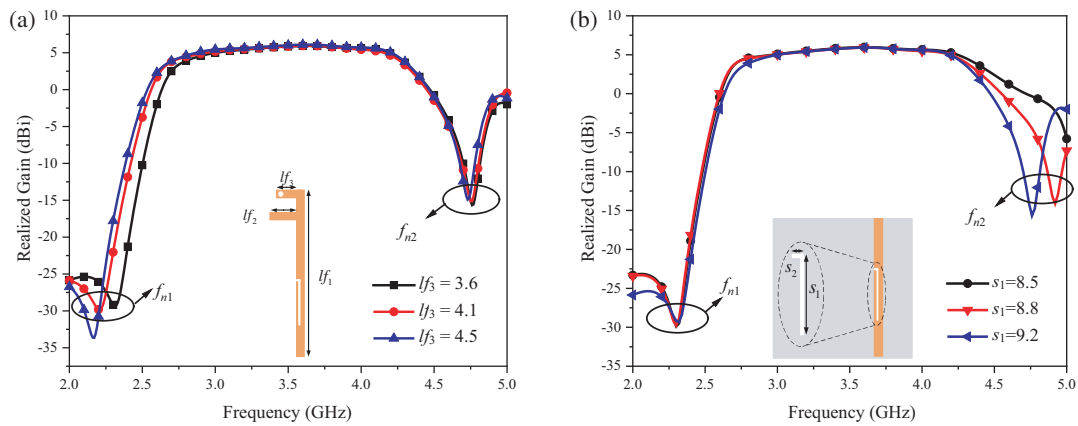


FIGURE 8. (a) Variation of realized gain with changing l_{f3} . (b) Variation of realized gain with changing s_1 .

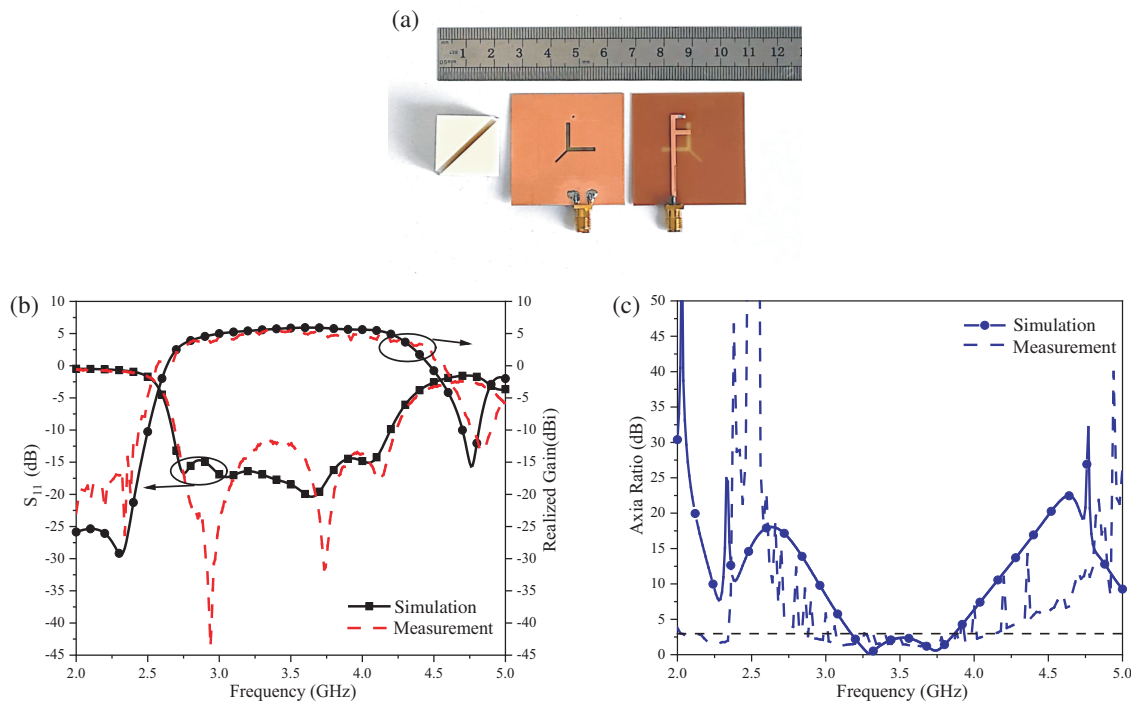


FIGURE 9. (a) View of the manufactured wideband CP FDRA. (b) Simulation and measurement of S_{11} and realized gain. (c) Simulation and measurement of ARs.

Through the parameterization of the proposed CP FDRA, the independent control of corresponding modes is achievable by adjusting the sizes of both the Y-shaped slot line and the DR. Furthermore, by adjusting the two radiation nulls flanking the passband, enhanced out-of-band selectivity is achievable.

3. MEASUREMENT RESULT

The proposed CP FDRA was fabricated and measured, and the fabricated antenna was measured using a vector network analyser (VNA). Fig. 9 presents the prototype of the antenna, as well as its simulation and measurement results.

It is noteworthy that the measurement results largely agree with simulation ones. The small deviations between the measurement and simulation results are mainly due to fabrication, assembly, and measurement. During the assembly process, the

air gap between the dielectric resonator and the ground plane will be formed due to the glue bonding, which will affect the energy coupling between the two. In addition, the placement of the dielectric resonator and the soldering of the joints will also affect the antenna measurement results. The antenna has a -10 dB impedance bandwidth of 46.1% (2.67–4.27 GHz) and an AR bandwidth of 23% (3.08–3.88 GHz). The averages of in-band realized gains for simulated and measured results are 5.4 dBi and 4.9 dBi, respectively. Furthermore, two radiation nulls are introduced at frequencies of 2.34 GHz and 4.86 GHz. These radiation nulls enhance the sideband roll-off rate, and the out-of-band suppression level exceeding 10 dB, thereby achieving a high-performance wideband CP FDRA, is obtained. The antenna radiation patterns at 3.28 GHz and 3.7 GHz are detailed in Fig. 10. As highlighted, the main radiation direction shows

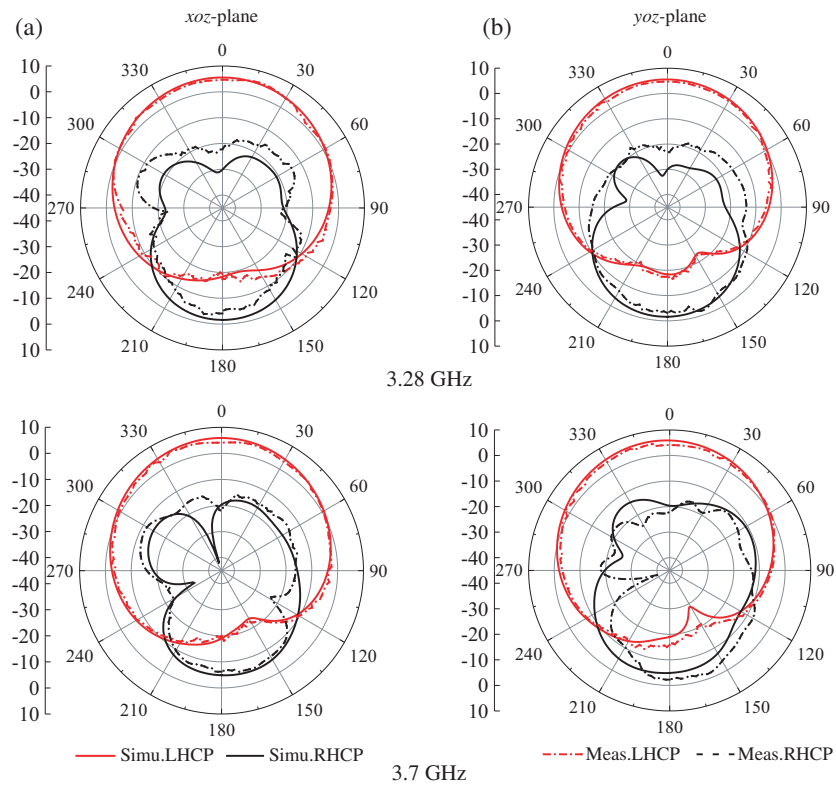


FIGURE 10. Radiation pattern of the wideband filtering DRA.

TABLE 2. Comparison with previous antennas.

Ref.	CF (GHz)	Pol.	Size ($\lambda_0 * \lambda_0 * \lambda_0$)	Impedance BW	AR.BW	Peak gain	Number of nulls
[8]	3.5	LP	$0.6 * 0.6 * 0.14$	21.1%	N.A	53 dBi	3
[9]	2.48	LP	$0.44 * 0.58 * 0.14$	18.5%	N.A	51 dBi	2
[18]	2.96	CP	$1.63 * 1.01 * 0.18$	13.5%	7%	6.2 dBi	0
[21]	3.6	CP	$0.96 * 0.96 * 0.14$	38.9%	34.3%	5.6 dBi	0
[22]	8.15	CP	$0.99 * 0.95 * 0.09$	6.13%	3.68%	5.3 dBi	2
[23]	2.44	CP	$0.89 * 0.89 * 0.15$	4.1%	4.9%	5.1 dBi	2
Prop.	3.47	CP	$0.46 * 0.46 * 0.18$	46.1%	23%	53 dBi	2

λ_0 is the free space wavelength at the center frequency

that the LHCP is 25 dB more potent than the RHCP. This confirms the antenna-dominant LHCP characteristic, which aligns well with the simulated findings.

Table 2 presents a comparative analysis of the previously published DRAs and the proposed antenna. It is evident that, compared with the filters proposed in [8] and [9], the antenna not only has a wider impedance bandwidth but also achieves a CP filtering effect. In comparison with the CP DRAs proposed in [18] and [21], the antenna integrates the filtering function while maintaining a wide impedance bandwidth and a 3 dB AR bandwidth. Furthermore, relative to other CP FDRAs introduced in [22] and [23], this antenna exhibits larger impedance and 3 dB AR bandwidths. The comparative analysis results show the antenna achieving a good balance in bandwidth, size, gain, and frequency selectivity.

4. CONCLUSION

In this paper, a wideband CP FDRA with filtering response is proposed. The wide impedance bandwidth and CP radiation are achieved by using a microstrip-Y-shaped slot line coupling feed structure. Two radiation nulls at the lower and upper passband edges are generated by the introduction of shorting stubs and spur lines on the microstrip feedline. The measurements show that the antenna has an impedance bandwidth of 46.1% (2.67–4.27 GHz), an AR bandwidth of 23% (3.08–3.88 GHz), and an in-band flat gain of 4.9 dBi. The antenna covers the 5G n78 and n79 bands, as well as the S band for satellite communications. It has broad applications in various domains, such as 5G mobile communications, radar systems, and satellite communications.

ACKNOWLEDGEMENT

This work was supported in part by the National Science Foundation of China under Grant 61661021 and 61901170, in part by the Natural Science Foundation of Jiangxi Province under Grant 20202BABL202008, Department of Education Science and Technology Program of Jiangxi Province under Grant GJJ2200609 and GJJ2200622.

REFERENCES

- [1] Pan, Y. M., P. F. Hu, X. Y. Zhang, and S. Y. Zheng, "A low-profile high-gain and wideband filtering antenna with metasurface," *IEEE Transactions on Antennas and Propagation*, Vol. 64, No. 5, 2010–2016, May 2016.
- [2] Chen, X., Q. Zhuge, G. Han, R. Ma, J. Su, and W. Zhang, "A wideband harmonic suppression filtering antenna with multiple radiation nulls," *Progress In Electromagnetics Research Letters*, Vol. 112, 17–25, 2023.
- [3] Petosa, A., *Dielectric Resonator Antenna Handbook*, Artech, 2007.
- [4] Ahmad, H., M. H. Jamaluddin, F. C. Seman, and M. Rahman, "MIMO dielectric resonator antennas for 5G applications: A review," *Electronics*, Vol. 12, No. 16, 3469, Aug. 2023.
- [5] Hu, P. F., Y. M. Pan, X. Y. Zhang, and S. Y. Zheng, "Broadband filtering dielectric resonator antenna with wide stopband," *IEEE Transactions on Antennas and Propagation*, Vol. 65, No. 4, 2079–2084, Apr. 2017.
- [6] Wang, C., Y. Zhang, Z. Han, G. Chen, X. Guan, and B. Ren, "A novel single-fed filtering dielectric resonator antenna using slotline-loaded coupling structure," *Microwave and Optical Technology Letters*, Vol. 64, No. 4, 750–754, Apr. 2022.
- [7] Liu, H., H. Tian, L. Liu, and L. Feng, "Co-design of wideband filtering dielectric resonator antenna with high gain," *IEEE Transactions on Circuits and Systems II: Express Briefs*, Vol. 69, No. 3, 1064–1068, Mar. 2022.
- [8] Ballav, S., G. A. Sarkar, and S. K. Parui, "High-selective filtering dielectric resonator antenna by integrating band-rejection resonators in feedline," *Sādhanā*, Vol. 46, No. 2, 1–8, Apr. 2021.
- [9] Wang, C., Z. Han, H. Liu, P. Wen, L. Wang, and X. Zhang, "A novel single-feed filtering dielectric resonator antenna using slotline stepped-impedance resonator," *IEEE Transactions on Circuits and Systems II: Express Briefs*, Vol. 68, No. 11, 3426–3430, Nov. 2021.
- [10] Liu, X., K. W. Leung, and N. Yang, "Frequency reconfigurable filtering dielectric resonator antenna with harmonics suppression," *IEEE Transactions on Antennas and Propagation*, Vol. 69, No. 6, 3224–3233, Jun. 2021.
- [11] La, D.-S., C. Zhang, Y.-J. Zhang, T.-X. Jiang, M.-J. Qu, and J.-W. Guo, "A wideband filtering dielectric resonator antenna based on the HEM_{11δ} mode," *IEEE Antennas and Wireless Propagation Letters*, Vol. 21, No. 8, 1552–1556, Aug. 2022.
- [12] Tang, H., L. Wu, D. Ma, H. Li, J. Huang, X. Deng, J. Zhou, and J. Shi, "Wideband filtering omnidirectional substrate-integrated dielectric resonator antenna covering Ku band," *IEEE Antennas and Wireless Propagation Letters*, Vol. 22, No. 7, 1746–1750, Jul. 2023.
- [13] Meher, P. R., B. R. Behera, S. K. Mishra, and A. A. Althuwayb, "A chronological review of circularly polarized dielectric resonator antenna: Design and developments," *International Journal of RF and Microwave Computer-Aided Engineering*, Vol. 31, No. 5, e22589, 2021.
- [14] Zhao, Z., J. Ren, Y. Liu, Z. Zhou, and Y. Yin, "Wideband dual-feed, dual-sense circularly polarized dielectric resonator antenna," *IEEE Transactions on Antennas and Propagation*, Vol. 68, No. 12, 7785–7793, Dec. 2020.
- [15] Liu, S., D. Yang, Y. Chen, S. Huang, and Y. Xiang, "Broadband dual circularly polarized dielectric resonator antenna for ambient electromagnetic energy harvesting," *IEEE Transactions on Antennas and Propagation*, Vol. 68, No. 6, 4961–4966, Jun. 2020.
- [16] Zhang, B., J. Ren, Y. Luan, J. Hou, and Y. Yin, "Three-port three-polarized dielectric resonator antenna with omnidirectional radiation," *IEEE Antennas and Wireless Propagation Letters*, Vol. 22, No. 12, 3122–3126, Dec. 2023.
- [17] Gupta, R. and A. Vaish, "Deminiaturized mode control rectangular dielectric resonator antenna," *Progress In Electromagnetics Research M*, Vol. 86, 173–182, 2019.
- [18] Yang, W.-W., W.-J. Sun, H. Tang, and J.-X. Chen, "Design of a circularly polarized dielectric resonator antenna with wide bandwidth and low axial ratio values," *IEEE Transactions on Antennas and Propagation*, Vol. 67, No. 3, 1963–1968, Mar. 2019.
- [19] Xu, H., Z. Chen, H. Liu, L. Chang, T. Huang, S. Ye, L. Zhang, and C. Du, "Single-fed dual-circularly polarized stacked dielectric resonator antenna for K/Ka-band UAV satellite communications," *IEEE Transactions on Vehicular Technology*, Vol. 71, No. 4, 4449–4453, Apr. 2022.
- [20] Yang, M., Y. Pan, and W. Yang, "A singly fed wideband circularly polarized dielectric resonator antenna," *IEEE Antennas and Wireless Propagation Letters*, Vol. 17, No. 8, 1515–1518, Aug. 2018.
- [21] Xia, Z.-X. and K. W. Leung, "3-D-printed wideband circularly polarized dielectric resonator antenna with two printing materials," *IEEE Transactions on Antennas and Propagation*, Vol. 70, No. 7, 5971–5976, Jul. 2022.
- [22] Chen, T.-W., W.-W. Yang, Y.-H. Ke, and J.-X. Chen, "A circularly polarized hybrid dielectric resonator antenna with wide bandwidth and compact size," *IEEE Antennas and Wireless Propagation Letters*, Vol. 22, No. 3, 591–595, Mar. 2023.
- [23] Caratelli, D., R. Cicchetti, V. Cicchetti, and O. Testa, "A wideband high-gain circularly-polarized dielectric horn antenna equipped with lamé-axicon stacked-disk lens for remote sensing, air traffic control and satellite communications," *IEEE Access*, Vol. 11, 20912–20922, 2023.
- [24] Sahoo, A. K., R. D. Gupta, and M. S. Parihar, "Circularly polarised filtering dielectric resonator antenna for X-band applications," *IET Microwaves, Antennas & Propagation*, Vol. 12, No. 9, 1514–1518, Jul. 2018.
- [25] Liu, Y.-T., K. W. Leung, J. Ren, and Y.-X. Sun, "Linearly and circularly polarized filtering dielectric resonator antennas," *IEEE Transactions on Antennas and Propagation*, Vol. 67, No. 6, 3629–3640, Jun. 2019.
- [26] Huang, T., H. Liu, H. Xu, and L. Geng, "3-D printed dual-band, dual-sense circularly polarized dielectric resonator antenna with a bandstop filtering response using planar via-free D-CRLH feeding network," *AEU — International Journal of Electronics and Communications*, Vol. 169, 154760, Sep. 2023.